PERGAMON

Electrochimica Acta 47 (2002) 1069–1078

ELECTROCHIMICA Acta

www.elsevier.com/locate/electacta

Improvement in the cycle life of LaB_5 metal hydride electrodes by addition of ZnO to alkaline electrolyte

Chunsheng Wang [a], Mariza Marrero-Cruz [a], Manuel P. Soriaga [a,*], Daniel Serafini [b], Supramaniam Srinivasan [c]

[a] *Department of Chemistry, Texas A&M University, Mail Stop 3255, College Station, TX 77843-3255, USA*
[b] *Physical Chemistry of Materials, Centro Atomico Bariloche, Bariloche, Argentina*
[c] *Center for Energy and Environmental Studies, Princeton University, Princeton, NJ 08544, USA*

Received 27 April 2001; received in revised form 8 August 2001

Abstract

The improvement in the cycle life of a metal-hydride electrode, $LaNi_{3.35}Co_{0.75}Mn_{0.4}Al_{0.3}$, brought about by the addition of ZnO to the alkaline electrolyte has been investigated using measurements based upon in situ electrical resistance, corrosion, scanning electron microscopy, X-ray photoelectron spectroscopy, X-ray diffraction and inductively-coupled plasma-atomic emission spectroscopy. It was found that Zn is underpotentially deposited on and subsequently alloyed with the subject electrode upon repeated charge-and-discharge cycles. The presence of Zn extends the cycle life of the $LaNi_{3.35}Co_{0.75}Mn_{0.4}Al_{0.3}$ electrode by inhibiting the disintegration and lowering the corrosion rate of the alloy particles.

Keywords: Ni-metal hydride electrodes; Ni-metal hydride batteries; LaB_5 metal hydride electrodes; $LaNi_{3.35}Co_{0.75}Mn_{0.4}Al_{0.3}$ alloys

1. Introduction

The use of metal hydrides (MH) as negative electrodes in alkaline rechargeable cells has become widely popular not only because of their high specific energy and energy density but also because of environmental concerns over conventional anode materials (e.g. Cd). An example is LaB_5 (where $B = Ni_{3.35}Co_{0.75}Mn_{0.4}Al_{0.3}$), an AB_5-type hydride electrode material based on $LaNi_5$ in which a fraction of Ni has been replaced with Co, Mn and Al. An important goal of an alloy modification is to improve the cycle life of the MH electrode.

The cycle life of a metal hydride electrode is limited primarily by the corrosion and disintegration (pulverization caused by hydrogen decrepitation) of the alloy; both serve to decrease the thermodynamic hydrogen absorption capacity of the alloy and increase the kinetic polarization during charge–discharge cycles [1–3]. Improved cycle life brought about by partial substitution of Ni with Co in $LaNi_5$ has been attributed to a reduced volume change during hydrogen absorption and desorption [3]. On the other hand, the high cycle life upon partial substitution of La by Ce in $LaNi_5$ alloys has been attributed to the formation of a passive CeO_2 film on the alloy surface [4].

It has recently been reported that improvements in the cycle life of LaB_5 electrodes can also be derived from the addition of: (i) ZnO in the electrolyte [5]; and (ii) Zn onto the alloys [6]. X-ray absorption near-edge structure (XANES) analysis of the Ni K-edge absorption indicated a significant decrease in the corrosion and/or buildup of $Ni(OH)_2$ in LaB_5 alloys when $Zn(OH)_4-$ ions are present in the electrolyte [7]. We have undertaken a more thorough investigation, via an arsenal of bulk and surface analytical methods, of the effect of the addition of ZnO to the alkaline electrolyte on the cycle life of LaB_5 hydride electrodes.

* Corresponding author. Tel.: +1-979-845-1846; fax: +1-979-845-3523.
E-mail address: m-soriaga@tamu.edu (M.P. Soriaga).

0013-4686/02/$ - see front matter
PII: S0013-4686(01)00801-5

2. Experimental

2.1. Preparation of alloy powders and electrodes

Alloy ingots of composition $LaNi_{3.35}Co_{0.75}Mn_{0.4}Al_{0.3}$ were prepared by arc melting a stoichiometric mixture of La, Ni, Co, Mn, and Al under an inert-gas (He) atmosphere. The ingots were pulverized into a powder, with particle size approximately 10 μm, by multiple iterations of $H_{2(g)}$ absorption and desorption. Electrodes were prepared by pressing 150 mg of a 50:50 weight mixture of alloy powder and binder onto a nickel mesh at a pressure of 300 kg/cm^2. The binding material was carbon (Vulcan-XC-72) with 33% polytetrafluoroethylene (PTFE). The working electrode had a surface area of 2 /cm^2.

2.2. Electrochemical charge–discharge cycling

All electrochemical experiments were conducted in a flooded, open cell containing 6 M KOH using electrochemical equipment by Arbin Instruments (College Station, TX). The counter electrode was a Ni mesh with a surface area tenfold greater than that of the working electrode. Potentials were measured with respect to a Hg/HgO reference electrode.

Cycle-life measurements were based upon a special charge–discharge procedure. The LaB_5 electrodes were first charged at a current of 100 mA/g for 3 h, and then equilibrated for 0.5 h. The electrodes were then discharged at a current of 50 mA/g to a cut-off potential of -0.6 V, and again equilibrated for 0.5 h. The purpose of the 0.5 h-equilibration time between charge and discharge was to measure the fully-charged and fully-discharged potentials at different charge–discharge cycles. Rate capabilities were measured at predetermined discharge currents, after the electrode was charged at a current of 100 mA/g for 3 h.

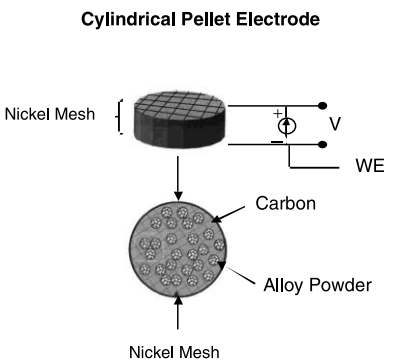

Fig. 1. Illustration of the Ni–metal hydride pellet electrodes used for in situ electrical resistance measurements.

2.3. In situ electrical resistance measurements

During the charge–discharge cycles, the alloy particles become pulverized and, hence disconnected, because of the volume difference between the metal and the hydride phases. The detachment of the active particles results in an increase on the electrical resistance of the electrode. Hence, the electrical resistance can be used as a measure of the degree of particle cracking during the charge–discharge cycles. For these experiments, a high (2:1) alloy-to-binder ratio was used; the electrode was fabricated by compression of the mixture between two nickel meshes at a pressure of 300 kg/cm^2. An illustration of the pellet electrode and the wiring connections for the electrical resistance measurements is shown in Fig. 1. In-situ electrical resistance of hydride electrodes was carried out using two potentiostats. One was for electrochemical hydrogen absorption–desorption, and the other was used for measuring electrical resistance by application of a constant current across the electrode. The metal-hydride 'sandwich electrode' was charged–discharged on one side only while a constant current of 10 mA was passed across it for electrical resistance measurements. The electrical resistance was extracted from the voltage drop across the two sides of the working electrodes. The electrical resistance thus determined refer to all physical elements of resistance present in the electrode, those include the electronic resistance of the series-parallel array of hydride particles, and various contact resistances not only between the particles themselves but also between the particles and the current collector.

2.4. Potential-composition isotherms

Electrodes were first fully charged at a constant current of 50 mA/g for 5 h. The room temperature equilibrium discharge potential-composition isotherms (PCI) were generated by a pulse discharge of 25 mA/g for 0.33 h, followed by a 0.33 h rest period until the potential remained unchanged. The time interval between successive dehydriding steps is critical: It should be long enough to ensure the establishment of equilibrium, yet short enough to prevent the loss of hydrogen by self-discharge. The total time for the measurements was close to 17 h; based upon the self-discharge data, the amount of desorbed hydrogen for this length of time was less than 3.5% of total amount.

2.5. XRD, SEM, XPS and ICP-OES measurements

X-rays diffraction (XRD) patterns were obtained using a Rigaku AFC5 diffractometer equipped with a rotating anode operated at 50 KV and 180 mA with a copper target and graphite-monochromated radiation. Scanning electron microscopy (SEM) images were ob-

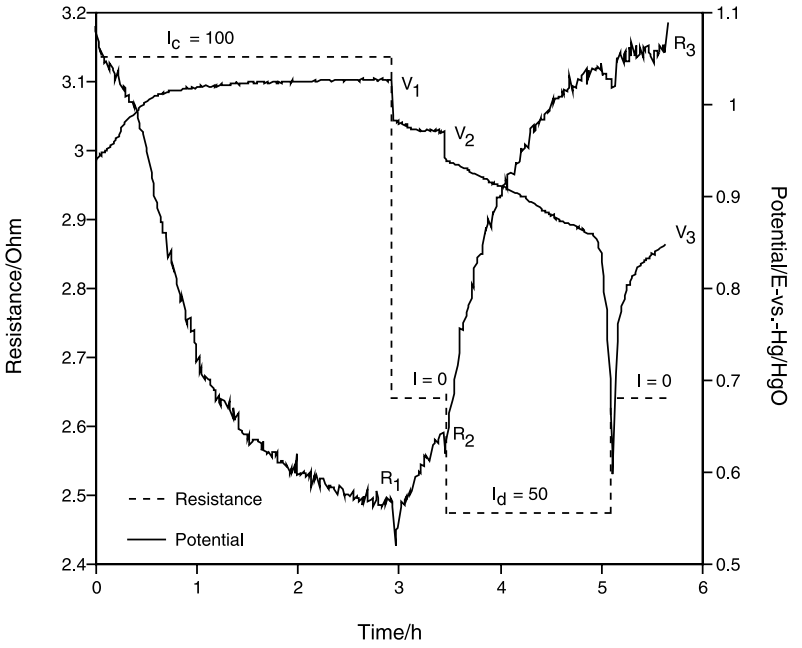

Fig. 2. Typical potential and electrical resistance changes of a $LaNi_{3.35}Co_{0.75}Mn_{0.4}Al_{0.3}$ electrode during one charge–discharge cycle in 6 M KOH + 0.5 M ZnO solution. Charge current: 100 mA/g; discharge current: 50 mA/g; rest period between charge and discharge: 30 min current for measuring electrical resistance: 10 mA. Indices 1, 2, and 3 in V and R serve to distinguish the different states of the electrode.

tained with a Jeol JSM-6400 microscope equipped with a Noran 1-2 energy-dispersive spectrometer (EDS). A 15-KV beam was employed to generate the back-scattered-electron images. X-ray photoelectron spectroscopy (XPS) were performed with a Perkin–Elmer PHI 5500 ESCA instrument equipped with 400-W monochromatic Mg Kα (1253.6 eV) and Al Kα (1486.6 eV) sources; only the former was used in the present study. A take-off angle of 42° and an instrumental resolution of 0.65 eV were employed. Elemental analysis for Ni corroded from the electrode into the alkaline electrolyte was carried out by inductively-coupled-plasma optical emission spectroscopy (ICP-OES) at the Department of Geology at Texas A&M University.

3. Results and discussion

3.1. Cycle life of $LaNi_{3.55}Co_{0.75}Mn_{0.4}Al_{0.3}$

Fig. 2 shows typical changes in the potential of the electrode in 6 M KOH + 0.5 M ZnO during one cycle of charge and discharge. The V_1 value represents the hydrogen-evolution potentials when the electrode was charged at a current of 100 mA/g. V_2 and V_3 are, respectively, open-circuit potentials of the fully charged, and fully discharged electrode after 0.5 h of relaxation.

The cycle-life of $LaNi_{3.55}Co_{0.75}Mn_{0.4}Al_{0.3}$ in 6 M KOH in comparison with that in 6 M KOH + 0.5 M ZnO is shown in Fig. 3. In order to understand the decline in capacity, the changes in V_1, V_2 and V_3 with cycle number is also given in Fig. 3. The arrows indicate the junctures at which the cell was disconnected to perform potential-composition-isotherm (PCI) and rate-capability measurements. From Fig. 3, it can be seen that the addition of ZnO to the KOH electrolyte has no effect on the maximum discharge capacity, but it does improve the cycle life. It can also be seen that the presence of ZnO inhibits the deterioration of the electrode after the PCI and rate-capability experiments.

Comparison of the V_1, V_2 and V_3 values for the ZnO-free and -added electrolyte, one finds: (i) V_1 of both cases first decreases and then increases. This can be explained by the breakdown of the surface oxide film (which leads to the decrease in V_1) when the particles expand/contract during the activation process; subsequent charge–discharge cycles then gradually forms a new oxide that results in the re-increase in V_1 [1]. A high V_1 value for the ZnO-added electrolyte during the initial (25) charge–discharge cycles is due to inhibition of hydrogen-gas evolution by electrodeposited Zn (vide infra); (ii) an almost invariant value of V_2 (ca. −0.93 V); this suggests that, after charging with only a current of 100 mA for 3 h, both electrodes are already fully charged; (iii) V_3 initially decreases and then becomes constant. The lower value of V_3 for the ZnO-added solution indicates that the presence of ZnO promotes an extensive discharge of the electrode.

The discharge capacity of alloys depends both on the thermodynamic hydrogen absorption capacity and the polarization kinetics for a given cut-off potential. The thermodynamic hydrogen absorption capacity can be

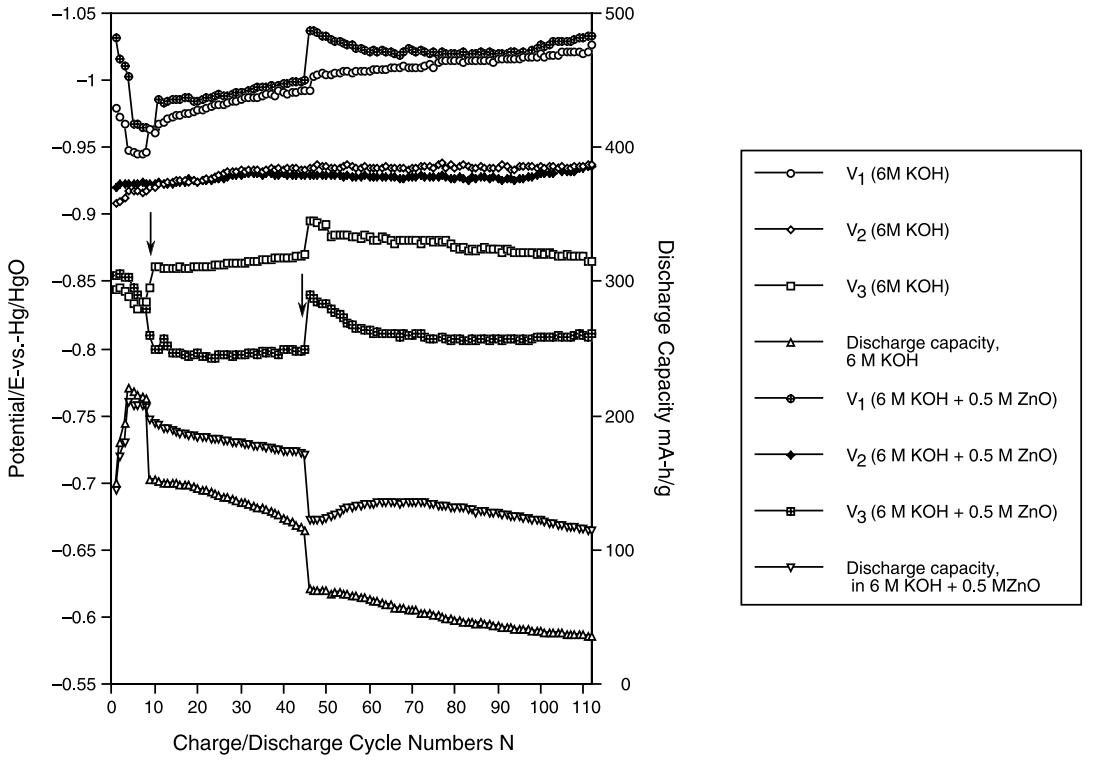

Fig. 3. Effect of the addition of 0.5 M ZnO to 6 M KOH solution on the cycle life of $LaNi_{3.35}Co_{0.75}Mn_{0.4}Al_{0.3}$ electrode. The arrows indicate stages at which the cell was disconnected for the performance of other experiments.

monitored by potential-composition isotherms (PCI), and the discharge kinetics can be (partially) evaluated by the rate capability. To understand the effects of ZnO in the electrolyte on the capacity stability of the metal-hydride electrode during charge–discharge cycling, the discharge PCI of the electrode at 8th and 45th cycles were measured, as shown in Fig. 4. After activation (8th cycle), only a slight decrease in the maximum hydrogen content is observed in the ZnO-containing solution; after 45 cycles however, the hydrogen absorption capacity in the ZnO-free solution becomes much lower than that in the ZnO-added electrolyte. A possible reason for this behavior is either: (i) a slow pulverization of the metal-hydride alloy particles; and/or (ii) a low corrosion rate and build-up of deposited Zn (vide infra). The scanning electron microscopy (SEM) images of electrodes with and without ZnO-additive after 115 charge–discharge cycles (Fig. 5) show a serious separation between the alloys and the carbon matrix, regardless of the composition of the electrolyte. In other words, ZnO in the electrolyte exerts little influence on the pulverization of the hydride particles. Hence, the high hydrogen absorption ability of electrode in ZnO-added solution may be attributed to a lower chance for the oxidation of the alloy particles and the build-up of deposited Zn; both of these result in small particle-to-particle and particle-to-current collector contact resistances. In such a case, an increase in hydrogen absorption capacity should be observed for ZnO-free solution after the pellet electrodes are re-pressed. Experiments were thus done in which the electrodes, subjected to 40 uninterrupted cycles in ZnO-free and Zn-added solutions, were removed and re-pressed at

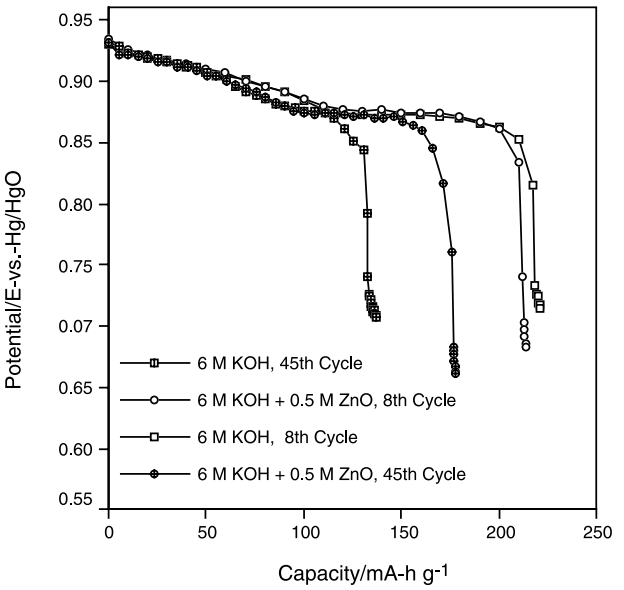

Fig. 4. Effect of the addition of 0.5 M ZnO additive to 6 M KOH solution on Potential-vs-Composition (in terms of capacity) curves after activation (8th cycle) and after prolonged cycling (45th cycle). The curves were measured during the discharge process.

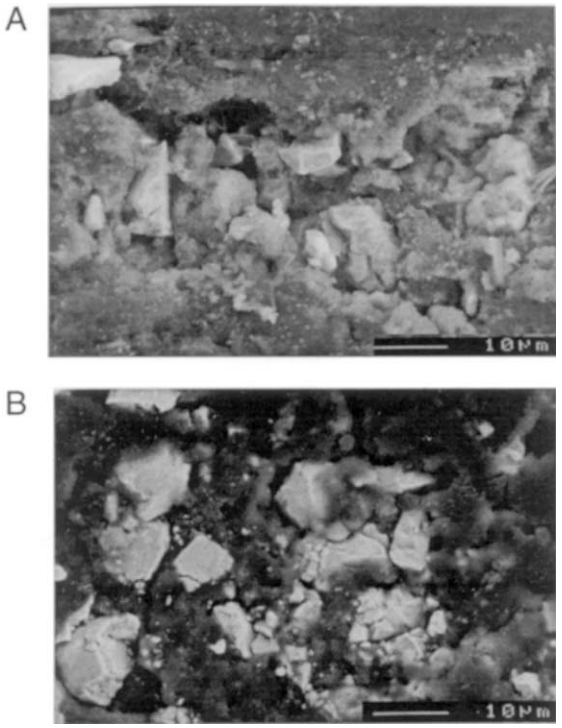

Fig. 5. Scanning electron microscopy images of the electrode after 115 cycles without (A) and with (B) ZnO added to the KOH electrolyte.

300 kg/cm^2 for 5 min. PCI measurements were then taken and the results are displayed in Fig. 6. As expected, the capacities of the re-pressed electrodes increased, with the increase much higher for the electrode that was exposed to the ZnO-free electrolyte.

Fig. 7 shows the effect of ZnO on the rate capability of the alloy electrode, at the 8th and 45th cycles, the rate capability of the electrode in the ZnO-added solution is lower than that in the ZnO-free electrolyte, a result that is probably due to the inhibition of hydrogen desorption by $Zn(OH)_4^{2-}$ ions in the solution. The inhibiting effects of $Zn(OH)_4^{2-}$ on hydrogen absorption/desorption has been confirmed by the lower polarization current in Tafel curves at the 8th cycle and at a 60% state of discharge, as shown in Fig. 8. Upon additional charge-and-discharge cycles (45th cycle), the rate capability increases in the presence of ZnO but decreases in the absence of ZnO Fig. 7, which is in agreement with the decrease in V_3 for electrode in ZnO-added solution Fig. 3. The increase in rate capability may be attributed to: (i) the disintegration of alloy particles, increasing the effective diffusion of hydrogen in the smaller particles; (ii) a decrease in the concentration of $Zn(OH)_4^{2-}$ ions due to underpotential deposition (UPD) and/or alloying of after numerous charge–discharge cycles (vide infra); (iii) corrosion inhibition and/or buildup of surface $Ni(OH)_2$ [7]; (iv) decreased resistance between alloy particles as a result of a build up of deposited Zn.

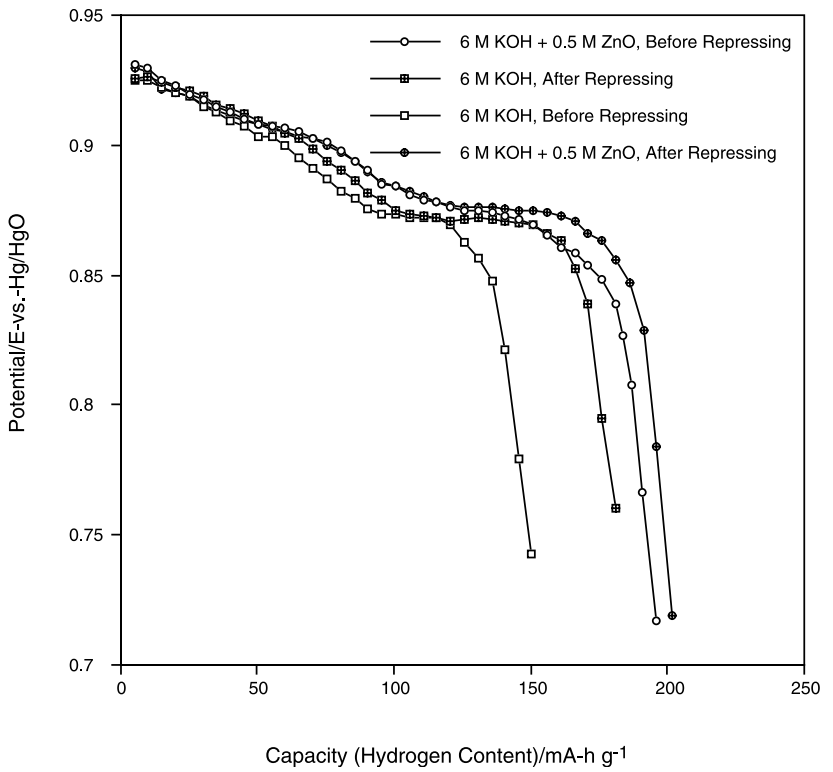

Fig. 6. Effect of re-pressing the electrode on the discharge PCI curves with and without ZnO added to the KOH electrolyte.

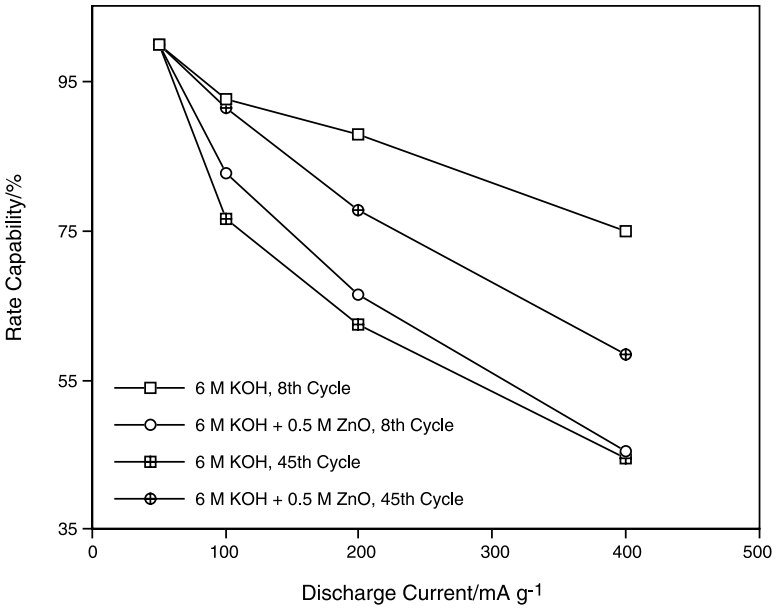

Fig. 7. Effect of the addition of 0.5 M ZnO additive to 6 M KOH solution on the rate capability of the electrode after activation (8th cycle) and after prolonged cycling (45th cycle).

3.2. In situ electrical resistance measurements

To directly monitor the particle-to-particle and particle-to-current collector contact resistances during charge–discharge cycles, an in situ electrical resistance measurement was carried out on the hydride electrode by application of a direct current across the electrode. The electrodes used in this particular phase of the study, prepared by the same method as the other electrodes, contained higher alloy-to-carbon ratio (2:1), and a higher total-mixture weight (0.225 mg) to facilitate the measurement of the electrical (internal) resistance (i.e. electrode disintegration).

A typical change in electrical resistance in the ZnO-added KOH solution, within a charge–discharge cycle is shown in Fig. 2. The R_1 value corresponds to the electrical resistance when the electrode was charged at a current of 100 mA/g (R_2) for 3 h. R_2 and R_3 are the electrical resistances of the electrodes at, respectively, fully-charged and fully-discharged states. During the 3 h of charging at a current density of 100 mA/g, the resistance decreased, accompanied by an increase in the amount absorbed hydrogen; these observations are due to the volume expansion of the alloy which improves the conductivity between the alloy and the carbon binder. When the changing current is suddenly terminated, the resistance drops off precipitously, initially to a low level at first, followed by a slight increase to a stable value. During the discharge process, the resistance increases due to volume contraction that inhibits conductivity between the alloy and carbon binder. Fig. 9 shows the changes in the electrical resistance and discharge capacity for an electrode in ZnO-containing electrolyte. It can be seen that the resistance initially increases quickly and then tapers off; this causes the discharge capacity to decrease fast, initially, and then to taper off. After 60 cycles, both the resistance and discharge capacity become stable. In order to investigate the influence of particle connectivity on the resistance, the electrodes were placed between two plastic plates and pressed after 78 cycles. It will be mentioned that the plastic plates have numerous tiny holes to enable electrolyte flow. After compression, the resistance was found to decrease from 2.77 to 0.165 Ω, and the discharge capacity was observed to increase from 85

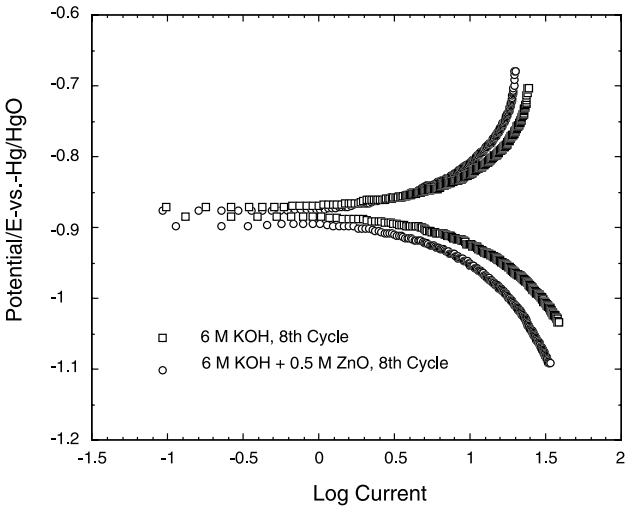

Fig. 8. Effect of the addition of 0.5 M ZnO additive to 6 M KOH solution on the Tafel polarization at 60% of the state of discharge after activation (8th cycle).

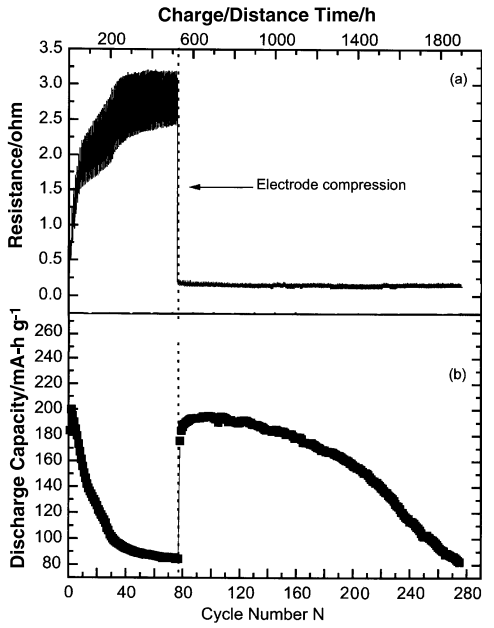

Fig. 9. Discharge capacity and electrical resistance changes of the test electrode during charge–discharge cycles in 6 M KOH + 0.5 M ZnO solution. The electrode was compressed by two plastic plates fixed by a screw after 78 cycles.

to 195 mAh/g. As charge–discharge cycling was continued, the discharge capacity decreased gradually, but the resistivity remained unchanged; this means that the oxidation of the alloy had become the critical step in the discharge capacity, if disintegration of electrode is non-existent.

Fig. 10 shows the time-dependence of the electrode electrical resistance before compression (at the 78th cycle) and after compression (at the 100th cycle) as indicated in Fig. 9. It can be seen in Fig. 10 that resistance drops to smaller values after compression, but the relative resistance change, $(R_3 - R_2)/R_3$, is essentially unchanged before and after compression (ca. 19%). This value is similar to the relative volume change (18%) of the $LaNi_{3.55}Co_{0.75}Mn_{0.4}Al_{0.3}$ alloy [7]. The relative change in resistance can thus also be used to monitor the relative changes in the volume of the alloy during the hydriding/dehydriding process.

Changes in the electrical resistance and discharge capacity of the electrode in ZnO-free electrolyte were also measured. The results are displayed in Fig. 11. At low compression applied during the first 95 cycles, the change in capacity was opposite of the resistance. At higher compression, after the 95th cycle, the resistance remained unchanged (Fig. 11). The calculated relative resistance from resistance change of pressed electrode at 105th cycle (Fig. 12) is 18%, similar to that in the ZnO-added electrolyte. The similar volume change during charge–discharge for ZnO-free and -added solution result in a similar pulverization behavior, which is in agreement with the previous SEM images after 115 cycles in ZnO-free and -added solution Fig. 5. Comparison of the capacities of the electrodes in the two electrolytes after high compression Figs. 9 and 11 re-

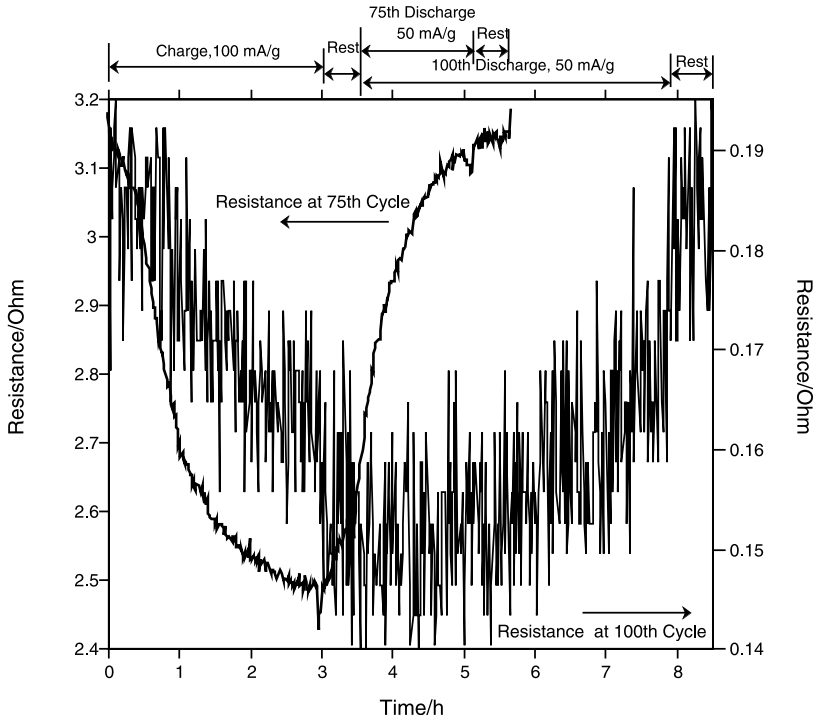

Fig. 10. Electrical resistance of electrode before compression (at 78th cycle) and after compression (at 100 cycle) in 6 M KOH + 0.5 M ZnO solution.

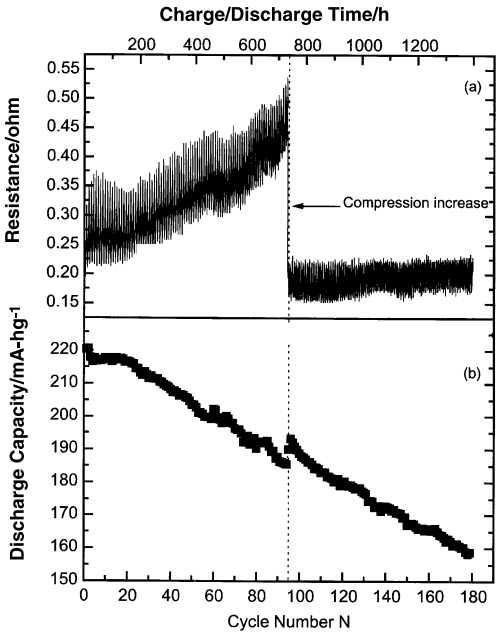

Fig. 11. Discharge capacity and electrical resistance changes of the sample electrode during charge–discharge cycle in 6 M KOH solution. The electrode was compressed by two plastic plates fixed by a screw; compression was increased after 95 cycles.

veals that the capacity decay in ZnO-added electrolyte is slower than that in ZnO-free electrolyte even if the electrical resistance is similar in both cases. This result provides further confirmation that the corrosion of alloy in ZnO-added solution is minimized, almost certainly because of underpotential deposition of Zn.

3.3. XPS, ICP-OES and XRD measurements

In order to confirm that Zn was underpotentially deposited during the charge–discharge cycles in ZnO-containing KOH electrolyte, X-ray photoelectron spectroscopy (XPS) and inductively-coupled plasma-optical

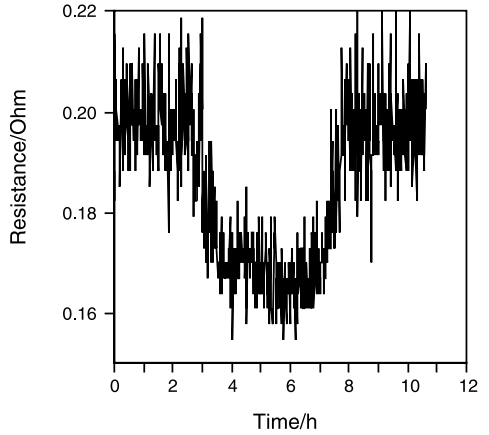

Fig. 12. The resistance change of pressed electrode during 105th charge–discharge cycle in 6 M KOH solution.

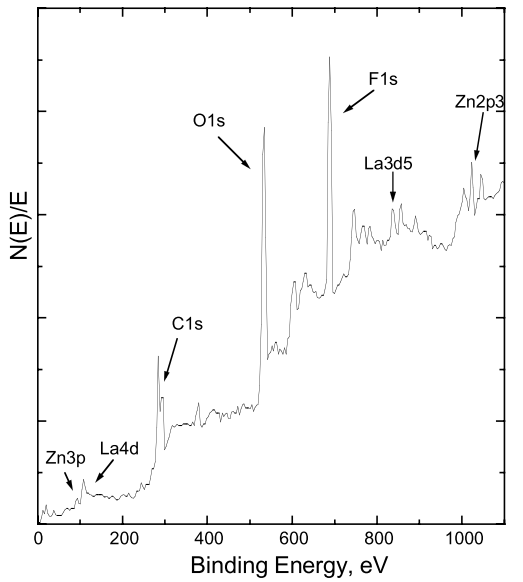

Fig. 13. Survey X-ray photoelectron scans of alloy electrode after 115 charge–discharge cycles. The C and F peaks are due to surface contamination from the binder.

emission spectroscopy (ICP-OES) were performed; the former was done for the electrode, whereas the latter was undertaken for the electrolyte. Fig. 13 shows a XPS survey scan of the alloy after 115 charge–discharge cycles. The presence of metallic Zn is indicated by the peak at 1021 eV, due to Zn $^2P_{3/2}$. A depth profile, in terms of Zn content as a function of sputtering time, is shown in Fig. 14. ICP-OES results of the Zn-containing electrolyte prior to and after 115 cycles showed a decreased, from 0.5 to 0.1 M in the ZnO content; the decreased is, of course, due to electrochemical deposition of Zn.

Fig. 15 shows the X-ray diffraction (XRD) patterns of the alloy powder after 115 cycles in ZnO-free and -added solution; the XRD patterns of the uncycled alloy and carbon powders are also shown for compari-

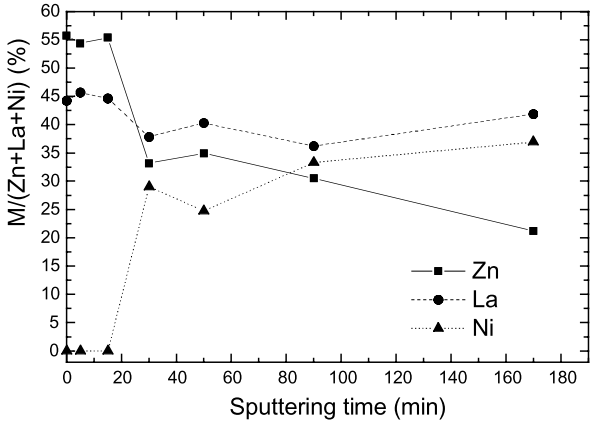

Fig. 14. XPS spectra of the alloy particles indicating Zn content at different sputtering depths.

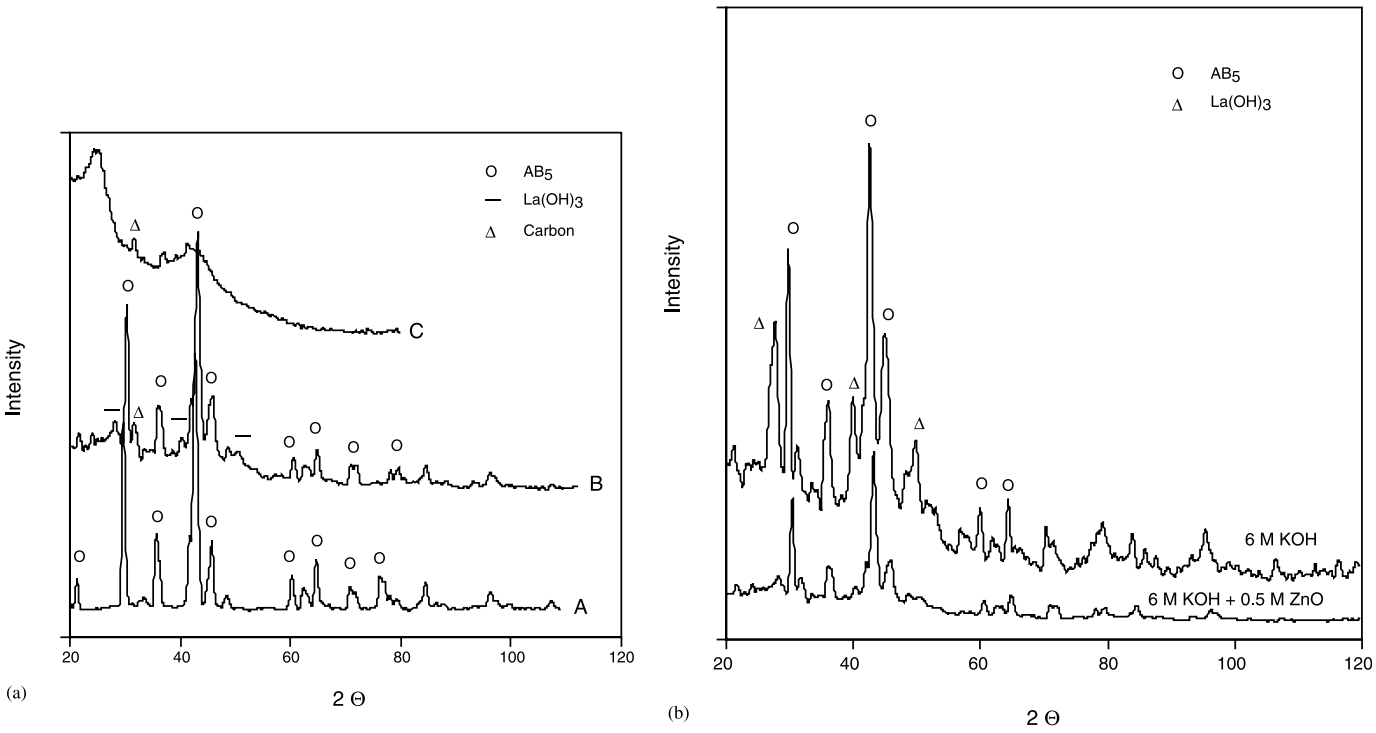

Fig. 15. (a) X-ray diffraction patterns of $LaNi_{3.35}Co_{0.75}Mn_{0.4}Al_{0.3}$: (A) alloy powers before charge–discharge cycles; (B) alloys mixed with carbon, after 115 charge–discharge cycles in 6 M KOH + 0.5 M ZnO solution; (C) vulcan-XC-72 carbon powder. (b) XRD patterns of $LaNi_{3.35}Co_{0.75}Mn_{0.4}Al_{0.3}$ mixed with carbon after 115 charge–discharge cycles in 6 M KOH with and without ZnO addition.

son. From Fig. 15, information can be extracted that shows the $LaNi_{3.55}Co_{0.75}Mn_{0.4}Al_{0.3}$ alloy having a $CaCu_5$-type phase. After 115 charge–discharge cycles, the $CaCu_5$-type structure is unchanged, but a small peak corresponding to $La(OH)_5$ emerges; hence, it can be argued that the alloy's internal crystallographic structure does not change even if its surface undergoes partial oxidation during charge–discharge cycles. Since the $La(OH)_3$ peak for the electrode cycled in ZnO-free 6 M LOH solution is higher than in ZnO-added solution, it can also be surmised that the formation of *surface* $La(OH)_3$ is inhibited by the presence of Zn. X-ray absorption near-edge structure measurements [7] showed that the Zn lowers the corrosion rate and the buildup of $Ni(OH)_2$ in $LaNi_{3.55}Co_{0.75}Mn_{0.4}Al_{0.3}$ alloys. In the present study, no peak that corresponds to $Ni(OH)_2$ has been observed; this is probably because of the low sensitivity of XRD methods for the detection of small amounts of $Ni(OH)_2$.

From the above XPS, ICP-OES and XRD results, it is clear that Zn is initially underpotentially deposited on the surface but is subsequently diffused into the bulk during charge–discharge cycles in ZnO-containing electrolyte. UPD Zn on the surface layer has no obvious influence on the volume change during the hydriding/dehydriding process. However, inhibition of the formation of $La(OH)_3$ by electrodeposited Zn can increase the conductivity of the oxides and/or retard the disintegration process. In both cases, the electrode cycle-life is enhanced.

4. Conclusions

The presence of $Zn(OH)_4^{2-}$ ions (0.5 M ZnO in 6 M KOH) can significantly improve the cycle life of $LaNi_{3.55}Co_{0.75}Mn_{0.4}Al_{0.3}$ electrodes. The improvement is brought about by: (i) the lower disintegration rate; and (ii) the lower corrosion rate of the hydride electrode. The first is due to UPD Zn that subsequently diffuses into the bulk; the second arises from inhibition of the build-up of $Ni(OH)_2$ and $La(OH)_3$.

Acknowledgements

This work was supported by the Chemical Sciences Division, Office of Energy Science, US Department of Energy, under contract DE-FG03-93ER14381.

References

[1] C.S. Wang, Y.Q. Lei, Q.D. Wang, Electrochim. Acta 43 (1998) 3193.
[2] C.S. Wang, Y.Q. Lei, Q.D. Wang, Electrochim. Acta 43 (1998) 3209.

[3] (a) J.J.G. Willems, Philips J. Res. 39 (1984) 1;
(b) J.J.G. Willems, K.H.J. Buschow, J. Less-Common Met. 129 (1987) 13.
[4] S. Mukerjee, J. McBreen, J.J. Reilly, J.R. Johnson, G.D. Adzic, K. Petrov, M.P.S. Kumar, W. Zhang, S. Srinivasan, J. Electrochem. Soc. 142 (1995) 2278.
[5] W. Zhang, H.F. Rogers, S. Srinivasan, The Electrochemical Society Meeting Abstracts, 96-1 (1996).
[6] W. Zhang, S. Srinivasan, T. Shen, R.B. Schwartz, The Electrochemical Society Meeting Abstracts, 96-2 (1996).
[7] S. Mukerjee, J. McBreen, G. Adzic, J.R. Johnson, J.J. Reilly, M.R. Marrero, M.P. Soriaga, M.S. Alexander, A. Visintin, S. Srinivasan, J. Electrochem. Soc. 144 (1997) L258.